MRS Advances © 2017 Materials Research Society
DOI: 10.1557/adv.2017.409

Silicon/polypyrrole nanocomposite wrapped with graphene for lithium ion anodes

Changling Li[1], Chueh Liu [1], Zafer Mutlu[1], Yiran Yan[1], Kazi Ahmed[2], Mihri Ozkan[2] and Cengiz S. Ozkan[1,3]
[1] Materials Science and Engineering Program, University of California Riverside, CA 92521
[2] Department of Electrical and Computer Engineering, University of California, Riverside, CA 92521
[3] Department of Mechanical Engineering, University of California Riverside, CA 92521

ABSTRACT

Herein, silicon nanoparticles (SiNPs) are coated with conducting hydrogel and wrapped with reduced graphene oxide (rGO) sheets via a facile and scalable solution-based sol-gel process. The in-situ polymerized polypyrrole (PPy) hydrogel forms an interconnected three-dimensional (3D) fiber matrix. Amine and hydroxyl groups from the hydrogel assist the encapsulation of the SiNPs through hydrogen bonding. The electro-conductive PPy fiber network and the wrapping of rGO offer efficient electron and ion transport pathways. The PPy/SiNPs/rGO electrodes can produce highly reversible capacities of 1312, 1285 and 1066 mAh g^{-1} at 100, 250 and 500 cycles at a current density of 2.1 A g^{-1}, respectively.

INTRODUCTION

The tremendous demand for improvement of electric vehicles (EVs) and plug-in hybrid electric vehicles (PHEVs) has promoted extensive research into new generation energy storage devices[1-4]. Silicon (Si) is considered to be a promising alloy anode material for the next generation lithium ion batteries (LIBs) and has been utilized in several commercial anodes[5, 6]. This is due to its low discharge potential relative to Li/Li^+ and the high theoretical capacity of 3572 mAh g^{-1} corresponding to the ambient temperature formation of a $Li_{15}Si_4$ phase[7]. However, Si suffers from poor capacity retention due to its large volume expansion in excess of 300% resulting from alloying with large amounts of Li during lithiation.

Nano-materials synthesized by advanced technologies, such as atomic layer deposition[8-10], electrospinning[11, 12], and self-assembly[13, 14] are used for the production of novel structures. Several nanostructured silicon and their composites such as SiNPs, double-walled Si nanotubes/nanowires, porous silicon have been verified to create the void spaces necessary for volume change during alloying and dealloying[15-17]. Moreover, silicon-carbon composites are proposed as high-performance anodes for LIBs[18-20]. Recently, gel-like conductive polymers, such as polyaniline (PANI) and PPy have adjustable conductivity and excellent mechanical properties[21]. Those polymers not only act as adhesive to bind Si but also offer continuous electro-conductive frameworks, which can substitute traditional resistive binders (e.g. polyvinlidene difluoride (PVDF), polyacrylic acid (PAA)) and carbon black.

In this work, we report on the synthesis of hierarchically nanostructured PPy hydrogel to encapsulate SiNPs with the wrapping of rGO sheets via a simple and scalable in-situ polymerization process. The continuous and seamless PPy coating wrapped with rGO sheets

produce an interconnected conductive framework, which is used to facilitate electron and Li-ion transport of the electrodes. Consequently, the rate capability of PPy/SiNPs/rGO is highly improved owing to the efficiently conductive PPy/rGO hybrid network. The LIB anodes based on PPy/SiNPs/rGO demonstrate an excellent reversible capacity of 1066 mAh g^{-1} over 500 cycles at a current density of 2.1 A g^{-1} (1C = 3.6 A g^{-1}). We believe this simple and energy-saving approach for synthesizing hybrid network based anodes offers a new method for large scale manufacturing battery devices.

EXPERIMENT

GO flasks were made using the improved Hummers' method[22]. The rGO wrapped PPy/SiNPs electrodes were prepared via a solution-based sol-gel polymerization process as follows: the phytic acid (50% wt.% in H_2O, Sigma Aldrich) was mixed with a pyrrole monomer (98 % reagent grade, Sigma Aldrich) in 0.8 ml isopropanol (IPA) to produce a gel in a molar ratio of 0.5:1 (phytic acid: 66.4 μL, pyrrole: 10.0 μL). 32.9 mg ammonium persulfate (APS) was dissolved in 0.3 ml deionized water, acting as an oxidant, and then added to the phytic acid/pyrrole solution and vortexed for 1 min for ample mixing. The molar ratio of phytic acid/pyrrole/APS is 0.5: 1: 1. After that, the solution was immediately transferred to a vial containing 60 mg Si nano-powder (Nanostructured & Amorphous Materials, Inc) and sonicated for 10 minutes at room temperature until the mixture became a viscous green solution. Then 0.4 ml rGO dispersion (2.5 mg/ml in IPA) was added to the above viscous gel-like solution and then vigorously stirred for 2 hours. Lastly, the formed hydrogel slurry was used to doctor-blade onto a Cu foil current collector and dried in vacuum overnight at room temperature (23 ^oC). The dried electrodes were gently rinsed with deionized water to remove undoped phytic acid and excess oligomers, then dried in vacuum.

The electrodes were prepared by doctor-blading a slurry on a pre-cleaned Cu foil with a pre-area mass loading of 0.5-1 mg cm^{-2}. A button-type (CR 2032) two-electrode half-cell configuration was used for the electrochemical measurements. Cells were assembled in an Argon-filled VAC Omni-lab glovebox with oxygen and H_2O level below 1 ppm. Pure Li metal was used as the counter electrode. A Celgard 3501 porous PP membrane was used as the separator. The electrolyte comprised of 1 M $LiPF_6$ in ethylene carbonate and diethyl carbonate (EC:DEC = 1:1, v/v) with additional 2% vol. vinylene carbonate (VC) additive. Cycling performance and galvanostatic charge-discharge were conducted on Arbin BT300 with a voltage window ranging from 0.01 to 1.0 V (vs. Li^+/Li). Capacity and C-rates were determined using 1C = 3.6 A g^{-1}. The capacities of this work were calculated based on the Si weight in the PPy/SiNPs/rGO composite. Cyclic voltammetry scans were tested at a fixed voltage window between 0.01 V and 1.0 V (vs. Li^+/Li).

DISCUSSION

Scanning electron microscopy (SEM) micrographs are shown to illustrate the structures and morphologies of the PPy/SiNPs/rGO composites in Figure 1a. Due to the existence of interactive hydrogen bonds and electrostatic interaction among the ternary components: SiNPs, porrole and phytic acid in the precursor, the polymerized PPy hydrogel produces a uniform

coating to encapsulate SiNPs. Before polymerization, the diameter of SiNPs ranges from 50 to 70 nm. A thickness of 10–20 nm of the gel-like conductive layer is formed to coat SiNPs, which is confirmed by an increase in the diameter of SiNPs to 80–90 nm after polymerization, as shown in Figure 1b. The PPy coating helps maintain the integrity of the solid electrolyte interface (SEI) layer during expansion. The PPy gel also generates a continuous conductive framework to shorten the electron and ion transport length while preventing SINPs detaching from the electrode. The rough surface has a 30–60 nm nano-scale pores which is assisted in the fast diffusion of Li-ion, and the micron pores alleviate the volume expansion of Si during lithiation (Figure 1b). It is worth noting that PPy/SiNPs are either wrapped inside the rGO sheets, or flatly covered by rGO on Si surface (Figure 1a-b). Therefore, rGO is able to improve the electrochemical stability of the network owing to its functional groups (e.g. carboxyl and hydroxyl) bonding with PPy/SiNPs surface. Furthermore, the outstanding conductivity of rGO can promote the electron and charge transfer, resulting in a higher rate capability.

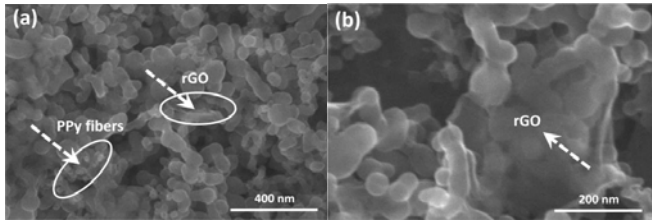

Figure 1. (a) Low magnification and (b) High magnification SEM micrographs of PPy/SiNPs/rGO.

X-ray diffraction (XRD) measurements were carried out to characterize the phase and purity of the as-prepared PPy/SiNPs/rGO composite (Figure 2). The PPy/SiNPs/rGO sample pattern exhibits narrow and sharp diffraction peaks, at 2θ of 28.6°, 47.7°, 56.4°, 69.4° and 76.4°, corresponding to the (111), (220), (311), (400) and (331) planes of Si crystals, respectively[23]. A relatively weak and amorphous scattering peak at 23.5° is observed in PPy/SiNPs/rGO spectra, representing the (104) crystal plane of PPy[24]. This implies the successful polymerization of PPy hydrogel coating for SiNPs for rGO spectra, a broad peak of around 24.6°, stemming from the partial restacking of exfoliated graphene layers, demonstrates the amorphous nature of the synthesized rGO[25]. The Si content in the composite was determined by Thermogravimetric analysis (TGA) in Figure S1.

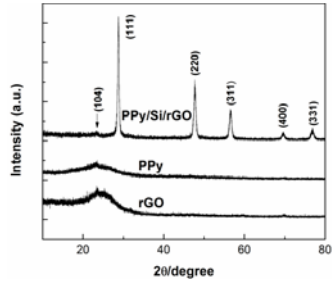

Figure 2. XRD patterns of SiNPs, pure PPy and PPy/SiNPs/rGO composites.

Galvanostatic charge-discharge and cycling performance is measured in a voltage range from 0.01 to 1 V (vs. Li^+/Li). Figure 3 demonstrates the rate capability of the PPy/SiNPs/rGO composite electrodes up to the 2.1 A g^{-1}, with additional cycling up to 500 cycles at 2.1 A g^{-1}. The 1st cycle is performed at 0.1 A g^{-1}, followed by 9 cycles at 0.2 A g^{-1} and 10 cycles at 0.4 A g^{-1}. This process is necessary for proper activation of the Si while fostering the formation of a stable SEI confirmed by above CV cycling measurements. The 1st discharge of the PPy/SiNPs/rGO electrodes exhibit a capacity of 3323 mAh g^{-1} and a charge capacity of 2639 mAh g^{-1}, corresponding to a Coulombic efficiency of 79.4 %. The applied potential range (1-0.01 V) for alloying lithium with silicon is beyond the lowest unoccupied molecular orbital (LUMO) of the carbonate based $LiPF_6$/EC electrolyte (~1V). Therefore, an amorphous SEI forms due to the reductive decomposition of the electrolyte during the lithiation of Si under the applied voltage. In the initial lithiation, the native oxide covering the surface of Si is destroyed and generates an inner SEI primarily composed of Li_xSiO_y and lithium ethylene dicarbonate (LEDC). An outer SEI mainly composed of LEDC and LiF forms as discharge continues. These SEI components containing lithium are stable under the applied potential window[26]. Thus, the consumed Li can't be extracted completely from the established SEI components during delithiation, which leads to the irreversible capacity loss and low Coulombic efficiency for the 1st cycle. After the kinetic enhancement is achieved via the activation process at three low current densities (0.1, 0.2 and 0.4 A g^{-1}) for the first 20 cycles, an integrated SEI is formed and the stabilized electrodes are cycled at a higher rate of 2.1 A g^{-1}. The PPy/SiNPs/rGO electrodes show reversible capacities of 1312, 1285 and 1066 mAh g^{-1} at 100, 250 and 500 cycles after being discharged at a high rate of 2.1 A g^{-1}. An average Coulombic efficiency (>99%) cycled at 2.1 A g^{-1} suggests the PPy/SiNPs/rGO anodes possess great stability and reversibility. In comparison, PPy/SiNPs without rGO sheets shows a capacity of 742 mAh g^{-1} after 500 cycles at 2.1 A g^{-1}, supporting that the addition of rGO highly improved the stability and rate capability of the electrodes. Galvanostatic charge/discharge curves are shown in Figure S2.

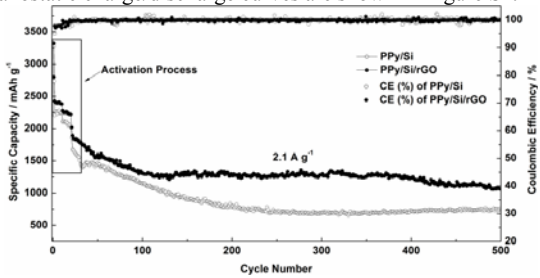

Figure 3. Cycling data and rate capability of PPy/SiNPs/rGO and PPy/SiNPs based anodes.

CONCLUSIONS

In conclusion, we have reported a highly scalable, cost-effective and environmentally benign synthesis route for producing PPy/SiNPs/rGO anodes with outstanding electrochemical performance over 500 cycles. The excellent performance of the anodes can be attributed to several factors including the hierarchical interconnected PPy framework, the conformal PPy

coating on SiNPs, and the incorporation of rGO sheets as the conductive additive for PPy/SiNPs electrodes. In addition, the solution-based synthesis process at room temperature offers a feasible alternative to the conventional slurry cast LIBs anodes by the substitution of non-conductive polymer binders and carbon black. The excellent electrochemical performance coupled with the highly scalable fabrication process allow this material to be a promising mass-fabrication of anodes for electric vehicle applications and portable electronics.

REFERENCES

[1] C. Liu, C. Li, K. Ahmed, Z. Mutlu, C.S. Ozkan, M. Ozkan, Sci. Rep. **6,** 29183 (2016).
[2] J.B. Goodenough, K.S. Park, J. Am. Chem. Soc. **135,** 1167 (2013).
[3] C. Liu, C. Li, K. Ahmed, W. Wang, I. Lee, F. Zaera, C.S. Ozkan, M. Ozkan, RSC Adv. **6,** 81712 (2016).
[4] C. Liu, C. Li, K. Ahmed, W. Wang, I. Lee, F. Zaera, C.S. Ozkan, M. Ozkan, Adv. Mater. Interfaces **3,** 1500503 (2016).
[5] X. Zhou, Y.-X. Yin, L.-J. Wan, Y.-G. Guo, Chem. Commun. **48,** 2198 (2012).
[6] O.K. Park, Y. Cho, S. Lee, H.-C. Yoo, H.-K. Song, J. Cho, Energy Environ. Sci. **4,** 1621 (2011).
[7] C. Li, C. Liu, W. Wang, J. Bell, Z. Mutlu, K. Ahmed, R. Ye, M. Ozkan, C.S. Ozkan, Chem. Commun. **52,** 11398 (2016).
[8] C. Liu, C.-C. Wang, C.-C. Kei, Y.-C. Hsueh, T.-P. Perng, Small **5,** 1535 (2009).
[9] L. Guo, X. Qin, F. Zaera, ACS Appl. Mater. Interfaces **8,** 6293 (2016).
[10] L. Guo, I. Lee, F. Zaera, ACS Appl. Mater. Interfaces **8,** 19836 (2016).
[11] C. Li, N. Chartuprayoon, W. Bosze, K. Low, K.H. Lee, J. Nam, N.V. Myung, Electroanalysis **26,** 711 (2014).
[12] L. Karen, C. Nicha, E. Cristina, L. Changling, B. Wayne, V.M. Nosang, N. Jin, Nanotechnology **25,** 115501 (2014).
[13] M.J. Maher, C.T. Rettner, C.M. Bates, G. Blachut, M.C. Carlson, W.J. Durand, C.J. Ellison, D.P. Sanders, J.Y. Cheng, C.G. Willson, ACS Appl. Mater. Interfaces **7,** 3323 (2015).
[14] L. Guo, F. Zaera, Nanotechnology **25,** 504006 (2014).
[15] N. Liu, Z. Lu, J. Zhao, M.T. McDowell, H.-W. Lee, W. Zhao, Y. Cui, Nat Nano **9,** 187 (2014).
[16] H. Kim, B. Han, J. Choo, J. Cho, Angew. Chem., Int. Ed. **47,** 10151 (2008).
[17] W. Wang, Z. Favors, C. Li, C. Liu, R. Ye, C. Fu, K. Bozhilov, J. Guo, M. Ozkan, C.S. Ozkan, Sci. Rep. **7,** 44838 (2017).
[18] A.G. Kannan, S.H. Kim, H.S. Yang, D.-W. Kim, RSC Adv. **6,** 25159 (2016).
[19] J. Chang, X. Huang, G. Zhou, S. Cui, P.B. Hallac, J. Jiang, P.T. Hurley, J. Chen, Adv. Mater. **26,** 758 (2014).
[20] T. Ni, L. Xu, Y. Sun, W. Yao, T. Dai, Y. Lu, ACS Sustain Chem Eng **3,** 862 (2015).
[21] K. Low, C.B. Horner, C. Li, G. Ico, W. Bosze, N.V. Myung, J. Nam, Sensor Actuat B: Chem **207, Part A,** 235 (2015).
[22] D.C. Marcano, D.V. Kosynkin, J.M. Berlin, A. Sinitskii, Z. Sun, A. Slesarev, L.B. Alemany, W. Lu, J.M. Tour, ACS Nano **4,** 4806 (2010).
[23] C. Liu, C. Li, W. Wang, M. Ozkan, C.S. Ozkan, Energy Technol. **5,** 422 (2017).
[24] J.-G. Wang, B. Wei, F. Kang, RSC Adv. **4,** 199 (2014).
[25] H.H. Bay, M. Ghazinejad, M. Penchev, I. Ruiz, Z. Mutlu, M. Ozkan, C.S. Ozkan, MRS Proc. **1451,** 51 (2012).
[26] C. Li, C. Liu, W. Wang, Z. Mutlu, J. Bell, K. Ahmed, R. Ye, M. Ozkan, C.S. Ozkan, Sci. Rep. **7,** 917 (2017).